*ECS Journal of Solid State Science and Technology*, **8** (9) P522-P526 (2019)
2162-8769/2019/8(9)/P522/5/$38.00 © The Electrochemical Society

# Crystallization Properties of $Mg_{35}Sb_{65}$/Sb Nanocomposite Multilayer Films for Phase Change Memory Application

**Song Sun,[1] Yifeng Hu,[1,2,z] Yongkang Xu,[1] Tianshu Lai,[3] and Xiaoqin Zhu[1,z]**

[1] *School of Mathematics and Physics, Jiangsu University of Technology, Changzhou 213000, China*
[2] *Key Laboratory of Semiconductor Materials Science, Beijing Key Laboratory of Low Dimensional Semiconductor Materials and Devices, Institute of Semiconductors, Chinese Academy of Sciences, Beijing 100083, China*
[3] *State-Key Laboratory of Optoelectronic Materials and Technology, School of Physics, Sun Yat-Sen University, Guangzhou 510275, China*

The phase transition properties of $Mg_{35}Sb_{65}$/Sb multilayer thin films were studied, including the crystallization mechanism, surface morphology, atomic bonding mode and adhesion strength. With the increase of the thickness of $Mg_{35}Sb_{65}$ interlayers, $Mg_{35}Sb_{65}$/Sb thin film had better thermal stability and lower electrical conductivity. The growth-dominated crystallization mechanism made $Mg_{35}Sb_{65}$/Sb have ultra-fast phase change speed. The subtle change on surface morphology was ascribed to the grain growth and interface stress during crystallization. The scratch test revealed the adhesion strength contrast before and after crystallization. This work showed that $Mg_{35}Sb_{65}$/Sb multilayer film was a potential material with fast speed and good thermal stability for phase change memory application.
 [DOI: 10.1149/2.0231909jss]

Manuscript submitted August 5, 2019; revised manuscript received August 20, 2019. Published September 4, 2019.

In recent years, the information is increasing rapidly due to the development of cloud computing, big data, Internet of things and mobile network. It makes it very imperative to develop a new type of non-volatile memory with high density, low power consumption and nanosecond speed. As one of the most promising memories, phase change memory (PCM) has attracted huge attention because of its high integration, fast speed, low threshold voltage and outstanding fatigue performance.[1,2] The basic storage principle of PCM is the reversible phase change between crystal state (low resistance state) and amorphous state (high resistance state) induced by a fast voltage pulse with different widths and heights.[3] Thus, the operations of writing ("1") and erasing ("0") can be realized.[4] This non-destructive reading process ensures an accurate readout of the stored information in PCM cells.[5,6]

Phase change materials play an important role in PCM.[7,8] There is a contradiction between the phase change speed and thermal stability for phase change materials. A high crystallization temperature will increase the operation power in SET process and slower the phase switching speed. Therefore, a balance should be found between the thermal stability and switching speed.[8] In present, the most widely used phase change material is $Ge_2Sb_2Te_5$ (GST) because of its commercial application in optical storage.[9] However, the thermal stability of $Ge_2Sb_2Te_5$ is relatively poor and the RESET power consumption is too high to meet the requirement for high-density storage.[10] Therefore, it is necessary to develop new phase change materials. The researches had shown that Sb has an ultra-fast phase transition rate while $Mg_{35}Sb_{65}$ (MgSb) has better thermal stability.[11] The nanocomposite of these two materials could manifest more of their integration and advantage complementation.[12] In this paper, the properties of MgSb/Sb composite films were studied. The phase transition mechanism, surface morphology, atomic bonding mode and film adhesion strength were investigated in details.

## Experimental

All films in this paper were prepared by magnetron sputtering. The cylindrical $Mg_{35}Sb_{65}$ target was placed in the A position while Sb target was placed in B target in vacuum chamber. The sputtering power of A, B target was fixed at 30W. The uniform film was formed by sputtering deposition on the surface of $SiO_2$ substrates in argon atmosphere of 0.4 Pa. The thickness of films was controlled by changing the sputtering time.[13,14] The composite films of MgSb/Sb were prepared by alternate sputtering $Mg_{35}Sb_{65}$ and Sb targets at room temperature. The total thickness of composite films was fixed at 50 nm. The sample plate was kept rotating of 20 r/m to guarantee the uniformity of the film during depositing. The electrical conductivity measurement system was built by cold/hot table (Linkam HFS600E-PB2) and tramegger (Keithley 6517B). The heating rate was 20°C/min. Atomic force microscopy (FM-nanoview1000 AFM) was applied to detect the surface roughness of the film during the phase transformation in a Semi-contact mode. The structure of thin films at different annealing temperatures was studied by Raman spectrum with the wavelength 514.5 nm. The scratch test was used to show the comparison of the adhesion strength between the film and the substrate.

## Results and Discussion

Fig. 1a showed the function between conductivity and temperature for four samples. The conductivity σ was obtained through the formula: $\sigma = 1/(dR)$, where $d$ was the thickness of the film and $R$ was the resistance of the film. It could be seen that the electrical conductivity increased gradually in heating process. An abrupt rise of conductivity was observed for all samples, which was caused by the transform from amorphous to crystalline state. The transformation temperature was defined as $T_c$. The $T_c$ for MgSb(1nm)/Sb(9nm), MgSb(3nm)/Sb(7nm), MgSb(5nm)/Sb(5nm) and MgSb(7nm)/Sb(3nm) were ~170, ~190, ~194 and ~199°C, respectively. The higher phase transition temperature $T_c$ usually meant better thermal stability. Literature showed that the phase transition temperature $T_c$ of GST was ~165°C.[15] Obviously, MgSb/Sb films had better thermal stability than GST. According to the equation:[16]

$$\sigma = \sigma_0 \exp(-E_\sigma/KT) \quad [1]$$

where $\sigma_0$ was a pre-exponential factor, $E_\sigma$ was the conductance activation energy, $K$ was the Boltzmann constant, and $T$ was the temperature, the relationship between film conductivity and reciprocal function of temperature for amorphous and crystalline states was obtained in Fig. 1b and 1c. At the amorphous state, the $E_\sigma$ increased from 0.22876 to 0.31181eV with the thickness of the MgSb interlayer. For the crystalline state, the $E_\sigma$ increased similarly from 0.04162 to 0.05667 eV. The value of $E_\sigma$ was about half of the band-gap according to the equation:[17,18]

$$E_\sigma = E_g/2 + \Delta E \quad [2]$$

where $E_g/2$ was the distance from the Fermi level to the conduction band and $\Delta E$ was the depth of the trap states. The increase of bandgap led to the decrease of carrier concentration, which was an important reason for the decrease of film conductivity after crystallization.[19] This finding was consistent with the trend of conductivity curves in Fig. 1a.

[z]E-mail: hyf@jsut.edu.cn; zxq@jsut.edu.cn

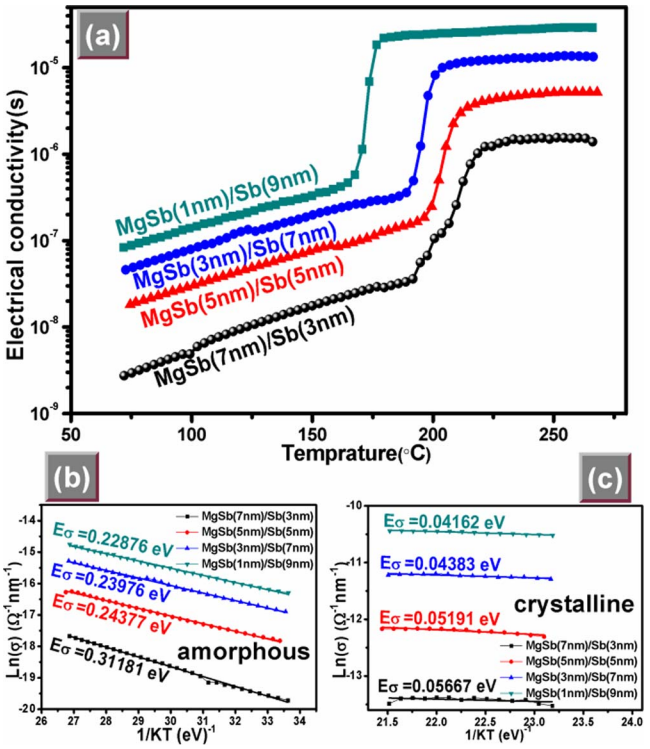


**Figure 1.** (a) Electrical conductivity as a function of temperature at a heating rate of 20°C/min for MgSb/Sb films. Arrhenius plots of ln(σ) versus *1/KT* for (b) amorphous and (c) crystalline MgSb/Sb films.

Data retention capability was an important parameter for phase change film. To obtain the failure time of the thin film, we selected four different isothermal temperatures for every MgSb/Sb thin film. Figs. 2a–2d showed the time dependent normalized resistance of MgSb/Sb films. It could be seen that the resistance of all thin films decreased with the increase of annealing time. The time when the resistance dropped to 50% of its initial value was defined as failure time. It was worth noting that at a lower annealing temperature the film had a longer failure time, because the film needed a longer time to accumulate enough energy for crystallization at a lower annealing temperature.[20] For MgSb(3nm)/Sb(7nm) thin film in Fig. 2a, the failure times of 20, 46, 95 and 532 s corresponded to the annealing temperature of 195, 190, 185 and 180°C, respectively. The similar results could be obtained for MgSb(5nm)/Sb(5nm), MgSb(3nm)/Sb(7nm) and MgSb(1nm)/Sb(9nm) films in Figs. 2b–2ad. In addition, the failure time increased with the thickness of MgSb layer at the same isothermal temperature 180°C (MgSb(7nm)/Sb(3nm)∼532 s, MgSb(5nm)/Sb(5nm)∼378 s, MgSb(3nm)/Sb(7nm)∼97 s). It revealed that the data retention capability of MgSb/Sb thin film could be improved by adding more MgSb ingredient.

The crystallization kinetics and behaviors of MgSb/Sb thin films could be investigated with the Johnson-Mehl-Avrami (JMA) theory.[21] In this paper, we assumed that the crystallization rate was proportional to the resistance change. The crystallization rate at any time was determined by the following equation:[22]

$$\chi(t) = (R_0\text{-}R_t)/(R_{max}\text{-}R_{min}) \quad [3]$$

Where $R_0$, $R_t$, $R_{max}$ and $R_{min}$ were the initial resistance, real-time resistance, maximum resistance and minimum resistance in the test process, respectively.[22] The fraction of crystallization $\chi(t)$ vs. time $t$ could be described by the following equation:[23]

$$\chi(t) = 1\text{-}exp[-(kt)^n] \quad [4]$$

where $n$ was the Avrami exponent and $K$ was an effective rate constant. In Fig. 3, the lower the annealing temperature, the longer the crystallization time. The typical *S*-shaped growth curves were observed, including incubation period, steady nucleation, growth and coarsening.[24] In the incubation period, the phase transition was time-dependent, which violated one of the assumptions of JMA theory, so this part of data must be removed from the JMA analysis.[24]

The curves of $Ln[-ln(1-\chi)]$ vs. $Ln(t)$ at different annealing temperatures were plotted in Fig. 4. The value of χ ranged from 0.10 to 0.70.

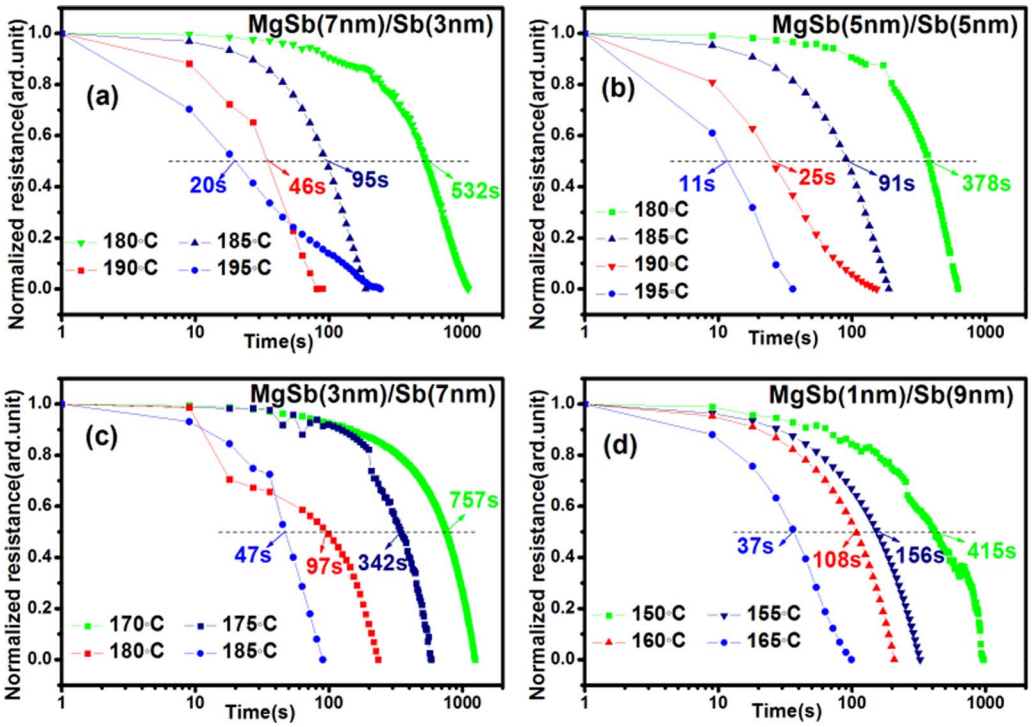


**Figure 2.** (a∼d) The change of normalized resistance with time for MgSb/Sb thin films at isothermal annealing process.

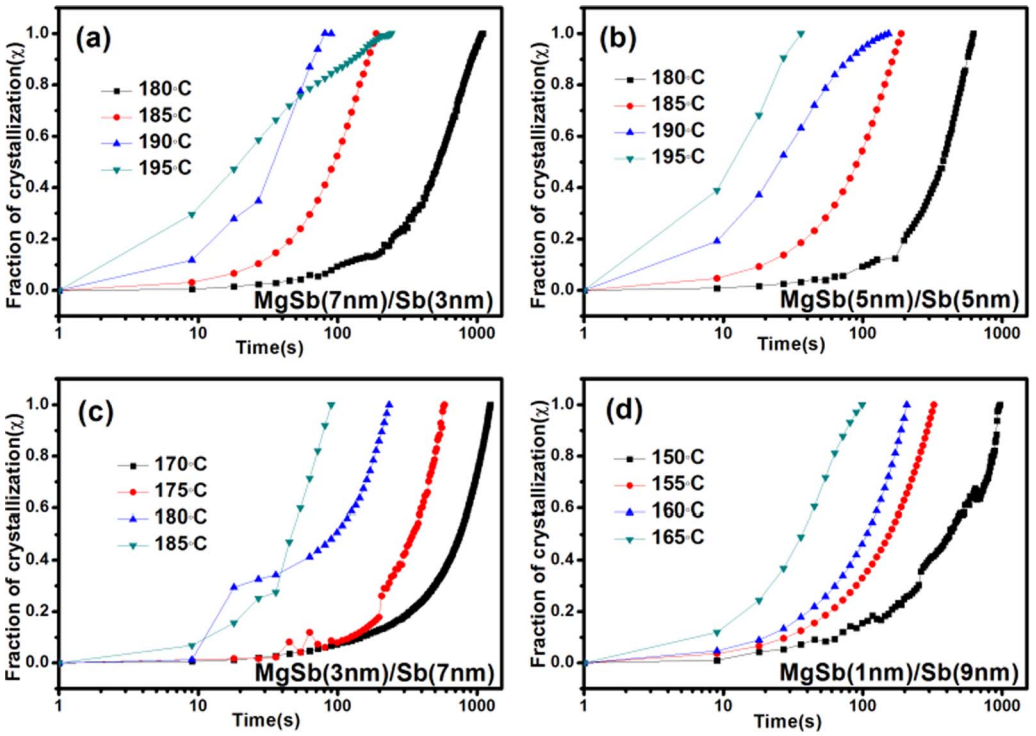


**Figure 3.** The fraction of crystallization as a function of annealing time for MgSb/Sb thin films.

The slope of the curve could be used to analyze the crystallization mechanism. In Fig. 4a∼4d, the linear fitting curves with the biggest slope were taken. The values of measured four slopes were all less than 1.5. Thus, it could be determined that the crystallization mechanism of MgSb/Sb thin film was one-dimensional growth-dominated.[20] This was very similar to the crystallization process of Sb-rich $Si_{16}Sb_{84}$[25] and $Ge_{15}Sb_{85}$[26] phase change films with good thermal stability and rapid crystallization rate.

Accompanied by the phase transition, the stress inside the film changed, which could lead to the change of the surface morphology. AFM images of MgSb(7nm)/Sb(3nm) film before and after crystallization were shown in Fig. 5. In amorphous state, the surface was smooth

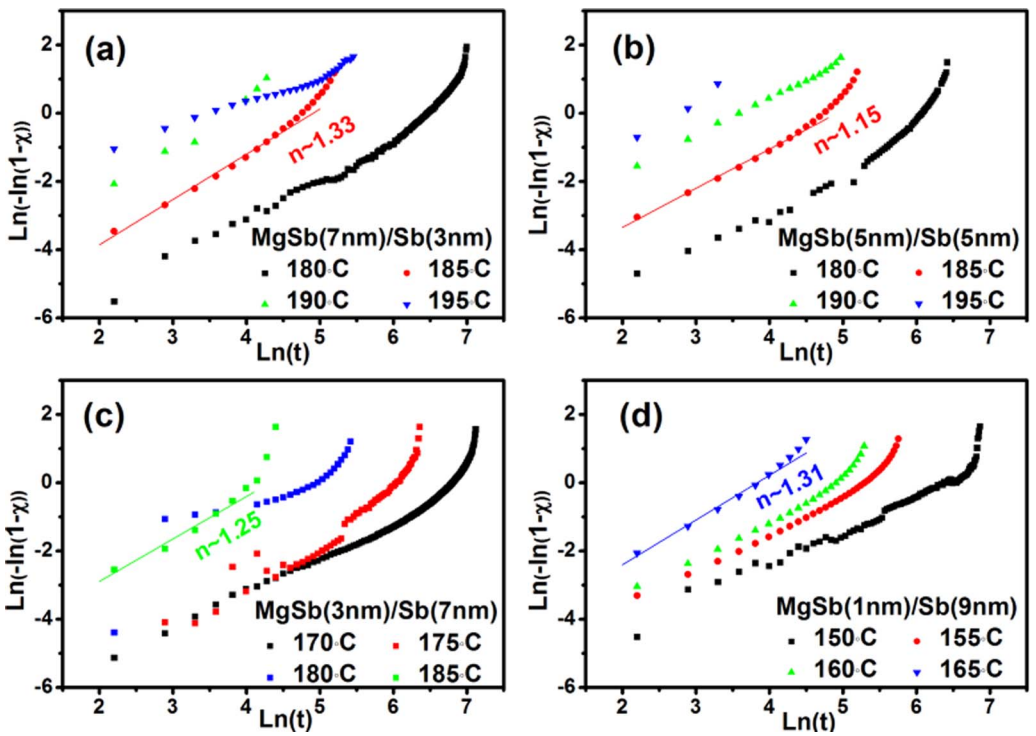


**Figure 4.** The relationship between *Ln[-ln(1-χ)]* and *Ln(t)* of MgSb/Sb films at different isothermal annealing temperatures.

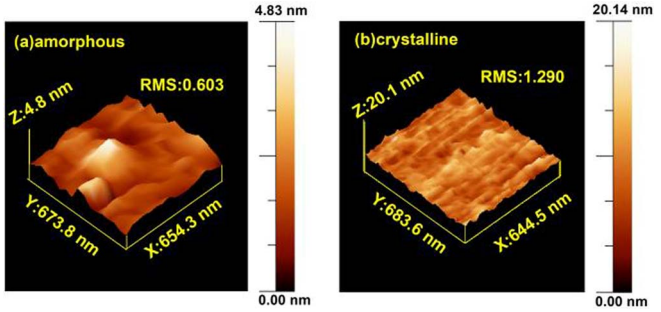


**Figure 5.** The AFM images of MgSb(7nm)/Sb(3nm) film for (a) amorphous state, (b) crystalline state.

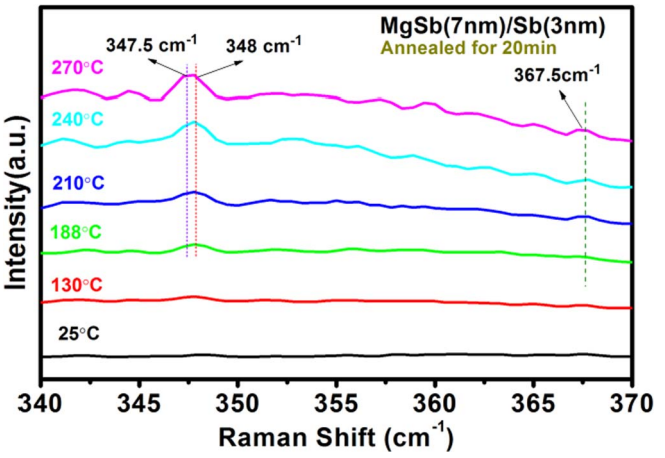


**Figure 6.** Raman spectra of MgSb(7nm)/Sb(3nm) films annealed at different temperatures.

with the root-means-square (RMS) surface roughness of 0.603 nm. After phase change, the RMS surface roughness increased a little to 1.290 nm. In amorphous state, the size of grains was small, resulting in a relatively smooth surface. After the crystallization, the grains grew, leading to the 'gully' surface as shown in Fig. 5b, so the RMS increased. On the whole, the difference was relatively small. The surface roughness of the phase-change film could affect the contact quality between the phase-change layer and the electrode in the PCM cell. It could be inferred that MgSb(7nm)/Sb(3nm)-based PCM device could have good reliability due to its smooth film surface.

The bond vibration modes and structural evolution were analyzed by Raman spectroscopy. Fig. 6 showed the Raman scattering spectrum of the MgSb(7nm)/Sb(3nm) films after annealing at 25, 130, 188, 210, 240, 270°C for 20 minutes. No peaks were observed below 130°C, indicating a typical amorphous structure. From above 188°C, a weak peak at around 348 $cm^{-1}$ appeared and became stronger with increase of annealing temperature. This peak was believed to originate from Sb-Sb octahedral vibrational mode.[27] After annealed at 270°C, this peak moved to a lower wavenumber of 347.5 $cm^{-1}$, which could be ascribed to the grain growth and stress effect. With the growing of grains in the thin film, the length of atomic bond increased due to tensile stress. The force constant of the film decreased and the vibration frequency of the atom decreased as well. It resulted that the peak of Raman spectrum moved to a lower wavenumber. In addition, a small peak at 367.5 $cm^{-1}$ maintained from 210 to 270°C.

The adhesion strength of MgSb(7nm)/Sb(3nm) films before and after crystallization were evaluated by scratch test. The micrographs of the film scratches were shown in Figs. 7a and 7c respectively. The movement of the diamond tip was from the left to the right during the scratch test. The scratch range was from 0 to 500 nm and the vertical load increased linearly from 30 to 100 mN. It could be clearly seen from the crack changes on the sample caused by scratches that the scratch for as-deposited thin film in Fig. 7a was deeper and wider than that of Fig. 7c, which might be due to the increased adhesion between the film and the silicon wafer after annealing. Figs. 7b and 7d showed the functional relationship between the acoustic emission (AE) signal of the sample and the loading force and the scratch distance. The red curve described the scratch distance under the vertical load, and the

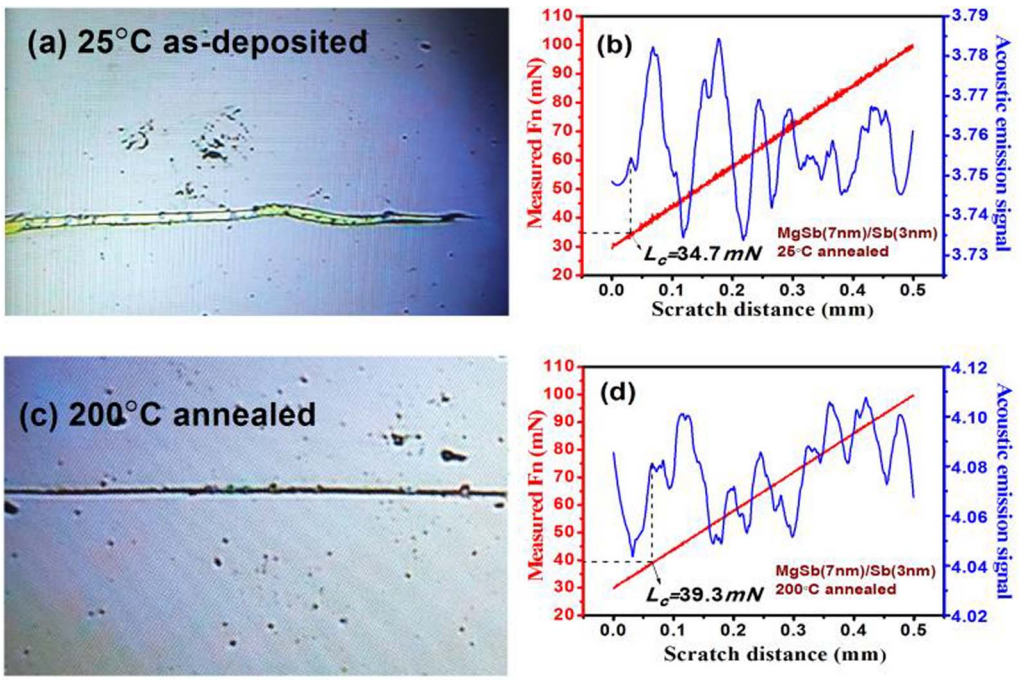


**Figure 7.** The scratch images for (a) as-deposited and (c) 200°C annealed MgSb(7nm)/Sb(3nm) film. The movement of the diamond tip was from the left to the right during the scratch test. The typical nano scratch test curves for (b) as-deposited and (d) 200°C annealed MgSb(7nm)/Sb(3nm) film with a maximum applied load of 100 mN.

blue curve described the AE signal. The point at which the film on the substrate began to layer and crack was called the critical point *C*. The vertical load at the point *C* was defined as the critical load $L_c$,[28] which could quantitatively characterize the adhesion strength between the thin film and the silicon wafer. As shown in Figs. 7b and 7d, the $L_c$ were 34.7 and 39.3 mN for as-deposited and 200°C annealed sample, respectively. The literature showed that the critical load $L_c$ for $Ti_8Sb_{92}$, $Ti_{27}Sb_{73}$, $Ti_{49}Sb_{51}$ films and $SiO_2$ were 5.8, 14.7 and 26.9 mN, respectively.[29] Therefore, MgSb(7nm)/Sb(3nm) film showed better adhesion strength than TiSb films.

## Conclusions

The behavior of crystallization of MgSb/Sb multilayer thin films were studied systematically. The results showed that the crystallization mechanism of MgSb/Sb film was one-dimensional growth-dominated. After phase change, the RMS surface roughness increased a little, which could be inferred that MgSb(7nm)/Sb(3nm)-based PCM device could have good reliability. The Sb-Sb octahedral vibrational mode was the main bond vibration mode. The adhesion strength of 39.3 mN demonstrated the excellent adhesion between the film and substrate.

## Acknowledgments

This work was supported by National Natural Science Foundation of China (No. 11974008, 11774438) and Changzhou key laboratory of high technology research (CM20173002) and the Opening Project of Institute of Semiconductors, Chinese Academy of Sciences (KLSMS-1805) and practice Innovation Program of Jiangsu Province (SJCX19_0712).

## ORCID

Song Sun https://orcid.org/0000-0001-9944-7192
Yifeng Hu https://orcid.org/0000-0001-7088-6829

## References

1. X. Ji, L. Wu, M. Zhu, F. Rao, Z. Song, Z. Hu, S. Guo, L. Xu, X. Zhou, and S. Feng, *RSC Advances*, **5**, 24966 (2015).
2. S. Raoux, F. Xiong, M. Wuttig, and E. Pop, *Mrs Bull*, **39**, 703 (2014).
3. G. Tianqi, S. Sannian, L. Le, S. Lanlan, W. Bingyao, L. Bo, S. Zhitang, Q. Ming, and F. Songlin, *Mater Lett*, **169**, 203 (2016).
4. Y. Lu, M. Stegmaier, P. Nukala, M. A. Giambra, S. Ferrari, A. Busacca, W. H. P. Pernice, and R. Agarwal, *Nano Letters*, **17**, 150 (2017).
5. W. Wu, Y. Hu, X. Zhu, Y. Sui, J. Xue, L. Yuan, S. Song, and Z. Song, *Journal of Materials Science: Materials in Electronics*, **26**, 9700 (2015).
6. H. You, Y. Hu, X. Zhu, H. Zou, S. Song, and Z. Song, *Journal of Materials Science: Materials in Electronics*, **28**, 10199 (2017).
7. X. Ji, L. Wu, W. Zhou, M. Zhu, F. Rao, Z. Song, L. Cao, and S. Feng, *Appl Phys Lett*, **106**, 023118 (2015).
8. Z. Xiaoqin, Y. Hu, J. Xue, Y. Sui, W. Weihua, L. Zheng, L. Yuan, S. Song, Z. Song, and S. Sun, *Journal of Materials Science: Materials in Electronics*, **25**, 2943 (2014).
9. D. Zhang, Y. Hu, H. You, X. Zhu, Y. Sun, H. Zou, and Y. Zheng, *Advances in Materials Science & Engineering*, **2018**, 1 (2018).
10. W. Weihua, Y. Hu, X. Zhu, Y. Sui, L. Yuan, L. Zheng, H. Zou, Y. Sun, S. Song, and Z. Song, *Journal of Materials Science: Materials in Electronics*, **27**, 2183 (2016).
11. S. Song, Z. Song, Y. Lu, B. Liu, L. Wu, and S. Feng, *Mater Lett*, **64**, 2728 (2010).
12. D. Loke, L. P. Shi, W. J. Wang, R. Zhao, H. X. Yang, L. T. Ng, K. G. Lim, T. C. Chong, and Y. C. Yeo, *Nanotechnology*, **22**, 254019 (2011).
13. K. Jiang, Y. Lu, Z. Li, M. Wang, X. Shen, G. Wang, S. Song, and Z. Song, *Materials Science and Engineering: B*, **231**, 81 (2018).
14. Z. Li, Y. Lu, M. Wang, X. Shen, X. Zhang, S. Song, and Z. Song, *J Non-cryst Solids*, **481**, 110 (2018).
15. Y. Hu, H. Zou, L. Yuan, J. Xue, Y. Sui, W. Wu, J. Zhang, X. Zhu, S. Song, and Z. Song, *Scripta Mater*, **115**, 19 (2016).
16. M. Zhu, L. C. Wu, F. Rao, Z. T. Song, X. L. Li, C. Peng, X. L. Zhou, K. Ren, D. N. Yao, and S. L. Feng, *J Alloy Compd*, **509**, 10105 (2011).
17. E. M. Vinod, K. Ramesh, R. Ganesan, and K. S. Sangunni, *Appl Phys Lett*, **104**, 063505 (2014).
18. H. You, Y. Hu, X. Zhu, H. Zou, S. Song, and Z. Song, *Applied Physics A*, **124**, 168 (2018).
19. C. Wang, J. Zhai, S. Bai, and X. Yao, *Mater Lett*, **64**, 2314 (2010).
20. H. Yifeng, X. Zhu, H. Zou, L. Zheng, S. Song, and Z. Song, *J Alloy Compd*, **696**, 150 (2017).
21. F. Rao, Z. T. Song, K. Ren, X. L. Li, L. C. Wu, W. Xi, and B. Liu, *Appl Phys Lett*, **95**, 032105 (2009).
22. H. Yifeng, Z. He, J. Zhai, P. Wu, T. Lai, S. Song, and Z. Song, *Applied Physics A. Materials Science & Processing*, **121**, 1125 (2015).
23. P. C. Chang, C. C. Chang, S. C. Chang, and T. S. Chin, *J Non-cryst Solids*, **383**, 106 (2014).
24. Y. J. Huang, T. C. Chung, C. H. Wang, and T. E. Hsieh, *J Electrochem Soc*, **157**, 113 (2010).
25. H. Huang, S. Li, F. Zhai, Y. Wang, T. Lai, Y. Wu, and F. Gan, *Mater Chem Phys*, **128**, 405 (2011).
26. Z. Wen, D. Wu, Y. Hu, A. Jiang, J. Xu, H. Liu, S. Bu, and R. Shi, *Journal of Materials Science Materials in Electronics*, **27**, 13148 (2016).
27. S. Sahu, R. Sharma, K. V. Adarsh, and A. Manivannan, *Appl Optics*, **57**, 178 (2018).
28. A. Feng, Y. Zhang, H. Xie, and Z. Fan, *Journal o f Jiang su University(N atural Science Edition)*, **24**, 15 (2003).
29. W. Wu, S. Chen, and J. Zhai, *J Mater Sci*, **52**, 11598 (2017).